Earth and Planetary Science Letters 506 (2019) 134–145

Contents lists available at ScienceDirect

Earth and Planetary Science Letters

www.elsevier.com/locate/epsl

An exceptionally weak Devonian geomagnetic field recorded by the Viluy Traps, Siberia

L.M.A. Hawkins [a,*], T. Anwar [b], V.V. Shcherbakova [c], A.J. Biggin [a], V.A. Kravchinsky [b], A.V. Shatsillo [d], V.E. Pavlov [d]

[a] Department of Earth, Oceans and Ecological Sciences, University of Liverpool, United Kingdom
[b] Department of Physics, University of Alberta, Edmonton, AB, Canada
[c] Geophysical Observatory "Borok IFZ RAS", Russian Academy of Sciences, Russian Federation
[d] Institute of Physics of the Earth, Russian Academy of Sciences, Russian Federation

ARTICLE INFO

Article history:
Received 23 February 2018
Received in revised form 19 July 2018
Accepted 24 October 2018
Available online xxxx
Editor: B. Buffett

Keywords:
paleomagnetism
paleointensity
geomagnetic reversals
GAD
Devonian
Viluy Traps

ABSTRACT

The detection of anomalous time averaged geomagnetic behaviour is crucial for understanding past magnetospheric shielding and inferring deep Earth evolution. Links have been suggested between geomagnetic field variation over timescales of tens to hundreds of millions of years and processes near the core–mantle boundary (CMB); however, this becomes difficult to establish prior to the Permo-Carboniferous Reversed Superchron (PCRS; 267–319 Ma) due to a lack of reliable data. To improve the record prior to the PCRS, we present multi-method produced paleointensity results from nines dykes and lava flows from the Viluy Traps, Siberia, emplaced during the Upper Devonian between 376.7 ± 1.7 Ma and 364.4 ± 1.7 Ma. These sites have previously been published as part of two paleodirectional studies, one of which produced the accepted 360 Ma pole for Siberia (Q factor 6). All of the sites produced very weak field values ranging from 4.3–14.9 ZA m^2, in close agreement with other recent results from Mid-Lower Devonian Siberian samples. Q_{PI} criteria have been used to illustrate the reliability of these new, low paleointensities, confirming the period of weak field suggested by other recent Siberian work, and the period of implied increased incidence of solar wind radiation, extended into the Upper Devonian. Along with evidence for moderate-high reversal frequencies and a potentially significant multipolar component during the Devonian, these weak field values also suggest a significantly different pattern of heat flow across the CMB relative to more recent times.

1. Introduction

The Earth's magnetic field is known to vary over timescales of tens to hundreds of millions of years, with potentially regular patterns in the variation of reversal frequency and field strength (Biggin et al., 2012). Three Superchrons have been identified during the Phanerozoic, with a periodicity of ~180 Myr (Pavlov and Gallet, 2005). It has been suggested that there is a relatively sharp transition going from higher than average reversal frequencies into these Superchrons; there is a peak in reversal frequency in the Jurassic, preceding the Cretaceous Normal Superchron (CNS), and there appears to be similarly high reversal rates during the Mid-Cambrian (Pavlov and Gallet, 2001), not long before the Ordovician Reversed Superchron (ORS). Reversal frequency and field strength may also be inversely coupled, with lower than average field strengths observed during the Jurassic peak reversal frequency while the CNS appears to have the highest field strength values of the Phanerozoic (Tauxe and Staudigel, 2004). However, the quality of the data during this time is not good enough to confirm this (Ingham et al., 2014).

All of these variations in field behaviour may be due to whole mantle convection mediating heat flow across the CMB, which in turn affects convection in the outer core. As well as fitting with the timescales over which these patterns of variation occur, this idea is supported by models showing that increased convection, above a critical value, increases reversal frequency and is coupled with a decrease in the dipole moment and a decrease in the dipolarity of the field (Olson, 2007). This class of models has also been used to directly show that increases in the total heat flow or changing the pattern of heat flow across the CMB results in increasing reversal frequency (Olson and Amit, 2014). Based on these relationships, paleomagnetism has the potential to provide an in-

* Corresponding author.
E-mail address: l.hawkins@liv.ac.uk (L.M.A. Hawkins).

https://doi.org/10.1016/j.epsl.2018.10.035

dependent record of changing CMB heat flux and the evolution of the deep mantle.

To confirm these patterns and their link to CMB heat flux, more reliable data are needed, especially preceding the PCRS. The geomagnetic field during this period, the Mid-Devonian to Early Carboniferous, is generally poorly understood due to the paucity of reliable data, including paleomagnetic poles (Torsvik et al., 2012), magnetostratigraphy (GPTS2016; Ogg et al., 2016) and paleointensity data (PINT15; Biggin et al., 2009). Recent work has tried to address this lack of data, including a magnetostratigraphic study by Hansma et al. (2015) on the Frasnian–Famenian of the Canning Basin. They reported a reversal frequency for this period of $\sim$2–5 Myr^{-1} based on the Oscar Range stratigraphy, similar to Palaeogene levels, which while lower than the peak in the Jurassic, would still be moderate to high compared to the rest of the Phanerozoic. This may also be an underestimate of the reversal frequency as there were reported sections with multiple neighbouring, single sample "chrons", which are not included in the calculated reversal frequency. While these could be excursions or possibly examples of onset delayed magnetisation, they may be periods of rapid reversals that are not fully captured because the sampling rate of one sample per 0.5–1 m is too low to capture the full number of reversals.

Recent work has also focused on improving the paleointensity record; there are only seven studies for the Devonian currently in the PINT15 database (Biggin et al., 2009) and the World Paleointensity Database (wwwbrk.adm.yar.ru/palmag/database_e.html). All of these studies reported low field values but, largely due to the age of these studies, they fall short of modern reliability criteria. Recent work on dykes and lava flows from the Minusa Basin, Siberia and the Kola Peninsula, support a weak field during the Lower–Middle Devonian (Shcherbakova et al., 2017). The five characteristic remanent magnetisation (ChRM) observed for the Minusa Basin samples, other than the expected 'N' and 'S' components, appear to be of primary Devonian age and suggest a significant multipolar component to the field during this time, fitting with field strength and dipolar contribution being coupled. Further work is needed, especially from the Upper Devonian, to a) explore if the palaeointensity and reversal frequency are coupled and b) to provide further evidence that the Devonian is similar to the Jurassic and incorporates a sharp transition in field behaviour preceding the PCRS, as observed during the late Jurassic–early Cretaceous before the CNS.

This study presents new, high quality paleointensities from Microwave Thellier-type, Thermal Thellier and Wilson techniques from the Upper Devonian Viluy Traps. These results are discussed in terms of their implications for Phanerozoic geomagnetic field variation and deep mantle evolution.

2. Geological background

The Viluy Traps is a Large Igneous Province (LIP), formed in association with the Viluy paleorift; the south-western branch of a 'triple junction' rift system that formed along the eastern margin of the Siberian Craton (Kravchinsky et al., 2002; Fig. 1). The associated magmatism comprises basalt flows within the rift basins, several NE-SW trending dyke swarms concentrated along the margins of the paleorift, associated sills towards the basin centre, kimberlites and alkaline ultrabasic rocks with carbonatites (Kiselev et al., 2012; Masaitis et al., 1975). The traps are known to be Late Devonian–Early Carboniferous in age from observed geological relationships; the dykes cut Middle to Late Devonian sediments, some are eroded and covered by Early Carboniferous sediments and clasts of trap materials are found in Early Carboniferous conglomerates (Kravchinsky et al., 2002). The initial age dating of the traps did not provide better constraints on their emplacement age as the majority of K–Ar age dates clustered between 340–380 Ma, with a scatter ranging from 450 to 320 Ma (Shpount and Oleinikov, 1987). More recent K–Ar and ^{40}Ar/^{39}Ar results from Courtillot et al. (2010) suggest that the emplacement of the traps occurred around the time of the extinction at the Frasnian–Famenian boundary (372.2 $\pm$ 1.6 Ma). Further work by Ricci et al. (2013) shows that the traps were probably emplaced in two stages; the first around the time of the extinction at 376.7 $\pm$ 1.7 Ma and then a second emplacement at 364.4 $\pm$ 1.7 Ma.

The samples used for paleointensity in this study were collected during two separate expeditions, as orientated blocks from exposures along the Viluy and Markha Rivers. Kravchinsky et al. (2002) published the paleodirections (Fig. 2) from the first expedition including dyke and sill samples from four sites from Markha River (sites M2, M4, M5, and M6) and three sites from Viluy River (V6-8), along with those from four kimberlite pipes of the Alakit–Markha region. The average direction from these sites (Ds = 319.1°, Is = −49.3°, $k = 31.5$, $\alpha_{95} = 8.3°$) was used to determine a pole position for the Siberian platform at $\sim$360 Ma, based on the age constraints available at the time. This pole is considered to be of high quality, with a Q factor of 6 (Torsvik et al., 2012) and several lines of evidence to suggest the directions from these sites are primary; the similarity between directions coming from different rock types (e.g. basalts and kimberlites), the sites being geographically disparate and the inclusion of a reversal.

The paleodirections from the second expedition were published by Orlov and Shatsillo (2011; Fig. 2); the sampling also took place along the Viluy River, from basalts from the upper part of the Emyaksinsk Formation, which are generally considered to be volcanic flows (Masaitis et al., 1975). These 12 sites (the VL sites) give paleodirections that are well clustered, with a reversed site in the sequence, giving an average direction of Ds = 191.6°, Is = 69.6° ($k = 80.4$, $\alpha_{95} = 4.9°$). While the majority of these paleodirections have the opposite polarity to those published by Kravchinsky et al. (2002), the two sets of directions do not pass a reversal test (Angle = 31.94°, Critical angle = 9.51°; Koymans et al., 2016; McFadden and McElhinny, 1990). They also plot closely to unpublished directions from sites (V1, 2 and 5) that were considered outliers in the study by Kravchinsky et al. (2002) because they were not antipodal to the majority of the directions.

There are several benign possibilities for why the paleodirections from these two studies are not antipodal; a time difference between the normal and reversed directions allowing for apparent polar wander (APW), unusual geomagnetic field behaviour, possibly from increased, long-lived non-dipole features, or the effects of palaeosecular averaging. The most recent age dating (Ricci et al., 2013) suggests that the traps were emplaced in two stages, $\sim$12 Myr apart, which could allow for APW, however there is no evidence to suggest any of the Viluy sites come from the earlier stage; The Vil sites and some of the V sites (V1, V2, V5 and V6) all come from the Appainsk and Emyaksinsk Formations, which have been dated to the second emplacement (from Vil 6 and Vil 13) but the other sites (V7 and 8) are not as well constrained and could have been emplaced earlier. There is the suggestion of a long-lived low intensity, multipolar magnetic field during the Devonian from Shcherbakova et al. (2017), however there is not the same strength of evidence for this from the Viluy sites. It has been noted, based on the high k for the upper part of the Emyaksinsk Formation, that the succession of lavas may have been emplaced coevally, although this is not supported by the reversed site in the succession. If this is the case, the Emyaksinsk Formation probably covers much less palaeosecular variation then the sites used for the 360 Ma pole (Kravchinsky et al., 2002). There is some support for this as the Vil sites do pass a reversal test at classification level C when compared to just the published and unpublished V sites

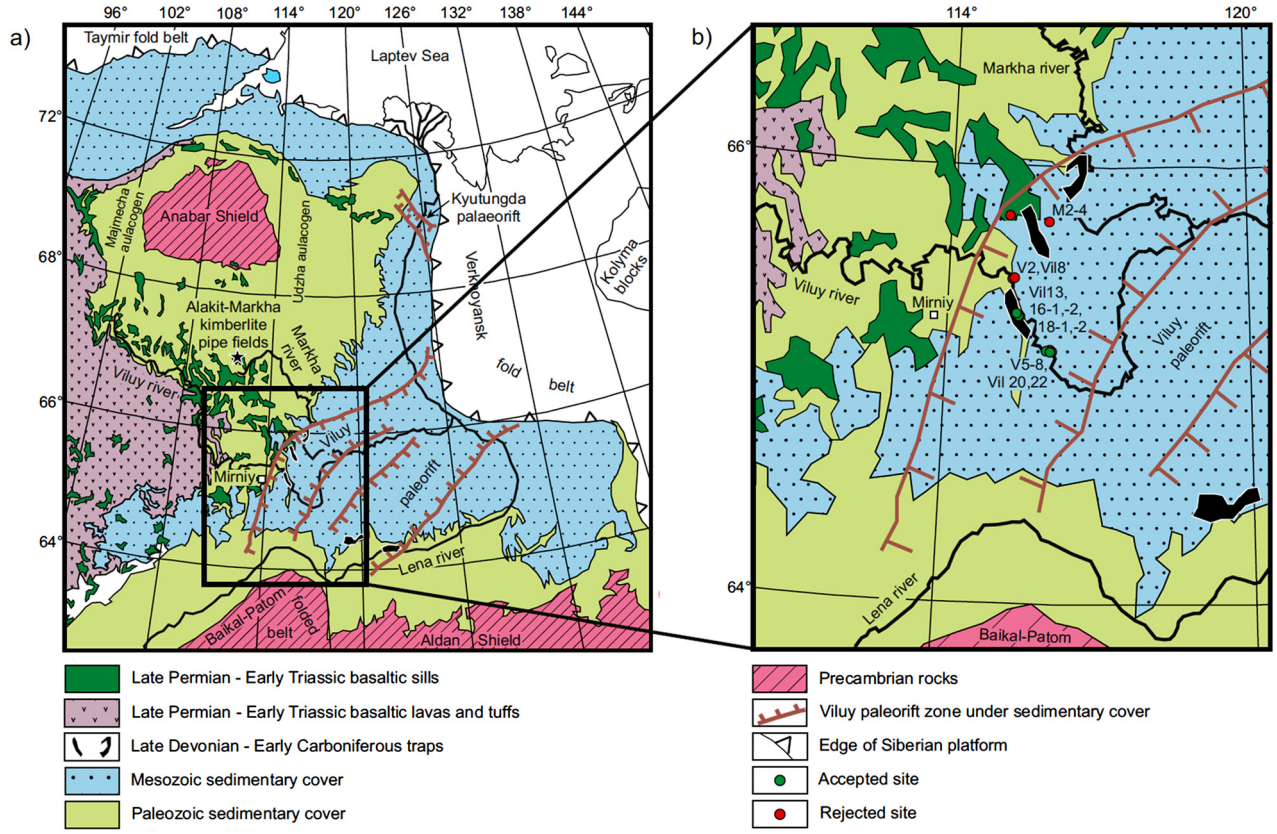

Fig. 1. a) Simplified geological map of the northeastern part of the Siberian platform from Kravchinsky et al. (2002); box shows the close up area shown on map 1b and b) Location of all of the sites used for palaeointensity from the two expeditions (Kravchinsky et al., 2002; Orlov and Shatsillo, 2011); sites that passed for paleointensity are shown in green, sites that failed are in red. (For interpretation of the colours in the figure(s), the reader is referred to the web version of this article.)

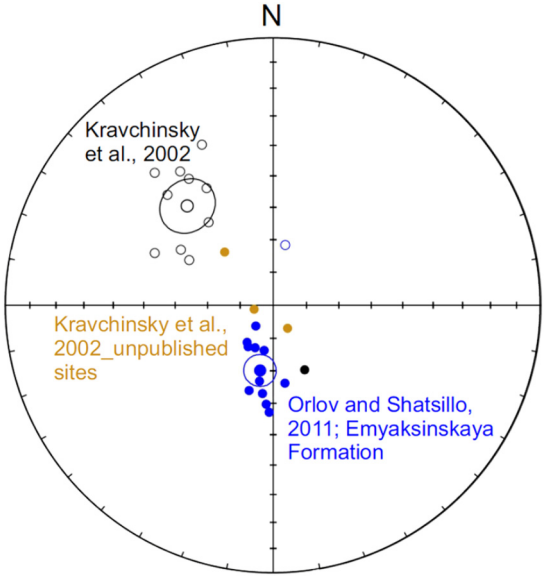

Fig. 2. Includes all the published VGP's from the Late Devonian–Early Carboniferous basalt flows and dykes from the Viluy and Markha river traps, as well as kimberlite pipes of the Alakit–Markha region considered to be of a similar age, used to produce the 360 Ma pole (black; Kravchinsky et al., 2002), three unpublished VGP's from the same study, originally considered to be outliers (brown; Kravchinsky et al., 2002) and the VGP's from the basalt flows of the Emyaksinskaya Formation (blue; Orlov and Shatsillo, 2011).

(Angle = 16.01°, Critical angle = 19.84°; Koymans et al., 2016; McFadden and McElhinny, 1990).

3. Magnetic mineralogy

Rock magnetic experiments were performed on at least one representative specimen from each site and, in conjunction with Scanning Electron Microscope (SEM) analysis, used to determine their magnetic mineralogy and suitability for palaeointensity experiments. The rock magnetic experiments were performed on crushed samples in air, using the Magnetic Measurements Variable Field Translation Balance (MMVFTB) at the University of Liverpool, to measure IRM, magnetic hysteresis properties and saturation magnetisation dependence on temperature. SEM analysis included Backscattered electron (BSE) imaging and energy dispersive X-ray (EDX) spectroscopy, performed on the carbon coated polished thin sections using a Zeiss EVO LS15 EP-SEM, operating at an acceleration voltage of 20 kV, at the Scanning Electron Microscope Laboratory of the University of Alberta. The combined analysis shows that samples with acceptable palaeointensity results can be divided into 3 magnetic mineralogy types, with some sites represented by more than one type (see Table 1).

Samples with type 1 magnetic mineralogy represent 37% of the samples that gave acceptable palaeointensity results. They display a single Curie temperature of ~580 °C and highly reversible saturation magnetisation curves upon heating and cooling up to 600 °C (Fig. 3a, b). This indicates that the samples are dominated by magnetite, with little to no titanium, and that the magnetic minerals in the samples are not altering during heating until above the Curie temperature. BSE imaging and EDX spectroscopy show that these samples contain bright, subhedral, titanium–iron oxides grains, up to ~60 μm in diameter, which are separated into two phases as multiple subsets of lamellae (Fig. 3c, d). These lamellae are characteristic of titanomagnetite that have undergone deuteric oxidation to form very low Ti titanomagnetite and ilmenite (Dunlop and

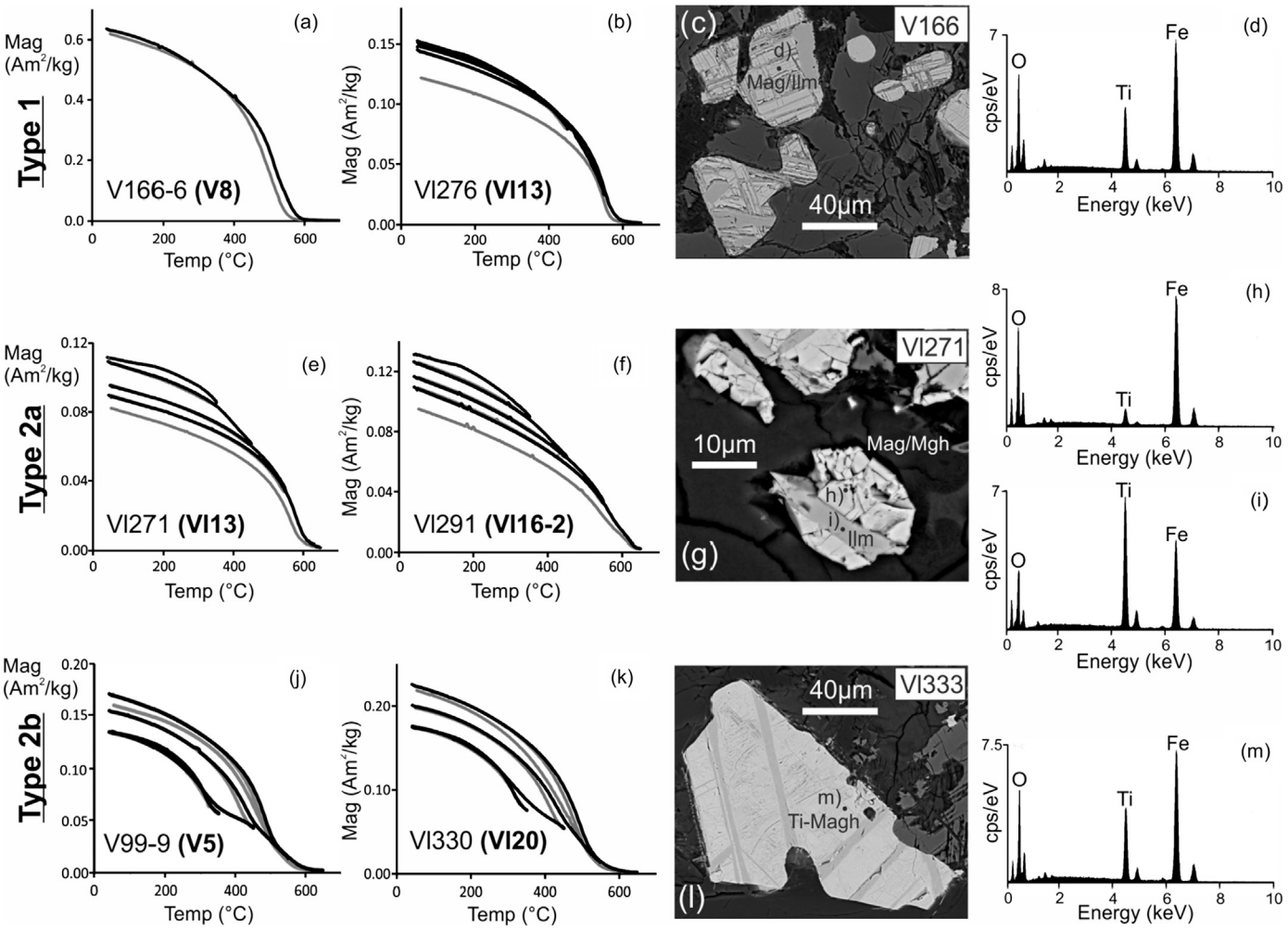

Fig. 3. Examples of saturation magnetisation with temperature curves, BSE images and EDX spectra for the 3 magnetic mineralogy types that pass selection criteria; a–d) Type 1, e–i) Type 2a and j–m) Type 2b. For the saturation curves, the first two columns, temperature steps of 100 °C between 350–650 °C were used for all of the experiments apart from a, which shows a single heating and cooling experiment to 700 °C. Black curves represent the heating steps, grey curves the cooling steps. For the SEM images, the third column, mineralogical abbreviations are: Mag, Magnetite; Ilm, Ilmenite; Ti-Magh, Titanomaghemite; Magh, Maghemite. The fourth column, the EDX spectra, shows the relative abundance of the iron oxide elements; O, Oxygen; Ti, Titanium; Fe, Iron.

Özdemir, 1997). On the Day plot (Fig. 4), the type 1 samples plot within the PSD region, largely around 50–60% on the SD–MD mixing line.

Samples with type 2 mineralogy represent 63% of the samples that gave acceptable palaeointensity results. All of the saturation magnetisation curves are irreversible from ~350 °C, indicating alteration occurs across all temperatures above this, however the samples can be divided into two sub-types. Type 2a samples give Curie temperatures between 580–650 °C (Fig. 3e, f), suggesting a mixture of magnetite, maghemite and possibly hematite (Dunlop and Özdemir, 1997), and the alteration from ~350 °C fits within the range of temperatures over which maghemite breaks down into hematite. Maghemite grains are apparently too fine to be observed directly using the SEM, however BSE images of magnetite–ilmenite lamellae (Fig. 3g) show signs of cracking which is commonly associated to the volume reduction associated with maghematisation (Dunlop and Özdemir, 1997). Hematite is also likely to be too fine to observe directly so it is difficult to distinguish if it is present originally or created by the transformation of the maghemite when heated. Type 2a samples plot further towards the SD region of the Day Plot then type 1, probably due to the SD maghemite/hematite present (Fig. 4).

Type 2b samples appear to contain two magnetic phases, one with a Curie temperature of 320–330 °C and the other between 520–580 °C (Fig. 3j, k). The higher Curie temperature is consistent with a very low-Ti titanomagnetite, while the lower Curie temperature would be consistent with a Ti-rich titano-magnetite. BSE imaging reveals bright, subhedral grains, up to ~170 µm in diameter, containing sparse lamellae (Fig. 3l). These suggest that there was originally some degree of exsolution, producing ilmenite, but the basalt likely cooled too fast or in insufficiently oxidising conditions, to allow the two phases to exsolve fully. Some of the irreversibility of the saturation magnetisation curves could be due to oxyexsolution of the titanomagnetite upon heating but these samples also appear to have been maghematised to titanomaghemite (the irregular, wavy structures on the titanomagnetite grains in Fig. 3l are an indication of shrinkage cracks). The type 2b samples also plot within the PSD region on the Day plot, between ~70–90% on the SD–MD mixing line (Fig. 4). The low degree of exsolution may explain the larger effective grain sizes of the type 2b samples than the type 1 samples. Palaeointensity estimates that passed our strict selection criteria have been retained despite having Type 2 mineralogy on the basis of them displaying minimal alteration of the remanence carriers as indicated by pTRM checks and their reliability in discussed sections 5.1 and 5.2.

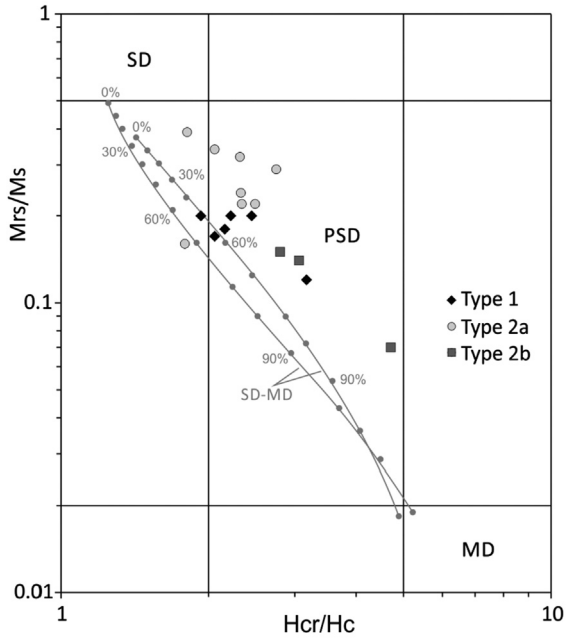

Fig. 4. Mrs/Ms vs. Hcr/Hc plot, based on Dunlop (2002), for all of samples that gave successful paleointensity determinations. Points are coded depending on their magnetic mineralogy type. Abbreviations are: Mrs, saturation remanence; Ms, saturation magnetization; Hc, coercivity; Hcr, coercivity of remanence; SD, single-domain; PSD, pseudosingle-domain; MD, multidomain. Includes the SD–MD mixture models for pure magnetite.

4. Paleointensity

4.1. Experimental technique

Four different palaeointensity methods were successfully used for determining palaeointensity; Microwave IZZI and perpendicular protocols, Thermal Thellier–Coe and Wilson. The bulk of the measurements were made on 5 mm, cylindrical samples, in air, using the 14 GHz microwave palaeointensity system with low-temperature SQUID magnetometer (Hill and Shaw, 1999) at the University of Liverpool, which has been demonstrated to give equivalent results to Thermal Thellier-style experiments (Biggin et al., 2007b). Almost all of the successful paleointensity determinations came from using the IZZI protocol (Tauxe and Staudigel, 2004); the samples are treated using Microwave energy in zero field and then in-field, before repeating these steps reversed at a higher power, with pTRM-checks made at each alternate power-time step. The experiment is conducted on individual specimens so the laboratory field could be varied each time to better fit the estimated paleointensity; in-field values ranged from 2–25 μT. In each case, the field was applied in a direction between 45 and 135° away from the ChRM such that a compromise was achieved between minimising any non-ideal behaviour arising from multidomain effects while also being able to detect its presence (Yu and Tauxe, 2005). The perpendicular protocol, without pTRM checks and tail checks, was also used (Hill and Shaw, 2007) but only gave one successful palaeointensity estimate.

Experiments on 1 cm cube specimens, using the Thellier–Coe method (Coe, 1967), were all undertaken at the University of Alberta (UofA) and the Geophysical Observatory 'Borok' of the Russian Academy of Sciences. At the UofA, samples were heated in a shielded ASC thermal demagnetizer and measured with a 2G cryogenic magnetometer. At Borok, experiments were conducted using with a full-vector three or two component vibrating sample magnetometer (3D-VSM or 2D-VSM), both of which were constructed at Borok with integrated furnace and magnetometer, or heated in an electric furnace and measured on an Agico JR6 spinner magnetometer. Specimens were heated twice in air: once in zero field and then again to the same temperatures, cooled in a laboratory field of 15 or 20 μT. These double heatings were carried out in over at least 12 steps up to 525–640 °C with pTRM checks and room-temperature susceptibility measurements performed after every second step and UofA included pTRM tail checks from 250–350 °C. No systematic variations in the palaeointensity results were observed between the different devices.

The selection criteria used for determining palaeointensity, taken from the Standard Palaeointensity Definitions (Paterson et al., 2014), are: $n \geq 4$; FRAC $\geq$ 0.25; $\beta \leq 0.1$; $q \geq 1$; $k' \leq 0.48$; MADanc $\leq 15°$; $\alpha \leq 15°$; DRAT $\leq$ 15% and CDRAT $\leq$ 15%. These are modified from the SELCRIT2 criteria (Biggin et al., 2007a) with the DRAT criterion relaxed because, in the majority of the cases, the overprint takes up a significant portion of the NRM and DRAT is normalized by the length of the best fit line and so CDRAT was added to help compensate for this relaxed criteria. PTRM tail checks were included for the majority of the Thermal Thellier experiments (excluding site Vil 22), while the Microwave used IZZI protocol in which MD behaviour is evident on the Arai plots as zig-zagging due to the alternating ZI and IZ steps (Riisager and Riisager, 2001). The curvature factor (Paterson, 2011) of the best-fit segment of the Arai–Nagata plot, k', has also been added to exclude MD behaviour.

Wilson's method (Wilson, 1961) was also applied to a select number of samples, using the 3D-VSM and 2D-VSM at the Borok observatory. For this technique, the curve produced by continuous thermal demagnetisation of the natural remanent magnetisation (NRM) is plotted against a full thermal remagnetisation curve (TRM) to find the temperature interval where the shape of the two curves is the most similar and used to calculate the palaeointensity. The similarity of NRM and TRM curves provides a strong argument in favour of the thermoremanent nature of the NRM and the Wilson method has an advantage of being independent of domain state. The samples were remagnetised in laboratory fields of 15 or 20 μT, the temperature interval selected was from between 150–600 °C and a published set of criteria for the selection of successful palaeointensity results, based on the degree of fit between the two curves (Muxworthy, 2010), were applied.

4.2. Palaeointensity results

Almost all microwave and thermal Thellier-type palaeointensity experiments produced two-slope Arai plots (Fig. 5), independent of the magneto-mineralogy type of the studied sample, while an example of the results from the Wilson technique is shown in Fig. 6. In the majority of cases, there is no significant change in the direction between the two slopes and the low power/temperature component satisfies the 15° criterion used for alpha. Site V7 is the exception, which shows an overprint in a >90° direction and a linear Arai plot once out of the overprint (Fig. 7b). All microwave and Thellier results passing the selection criteria, including those for the low temperature slopes, are listed in Supplementary Appendix A and Wilson results with selection criteria are listed in Supplementary Appendix B. However, while both the low and high temperature slopes for the Arai plots have been shown to pass selection criteria, in some cases for the same Arai plot, only the high temperature slopes were accepted as reliable for reasons that will be discussed in section 5.1.

Palaeointensity experiments were performed on 146 specimens from 17 sites, with 51 specimens from 9 sites producing reliable palaeointensity estimates, as summarised in Table 1. The paleointensity estimates range from 1.4–14.4 μT. An example of a failing Arai plot is illustrated by Fig. 5e; for the IZZI protocol, the Arai plots and Zijderveld diagrams show signs of zig-zagging indica-

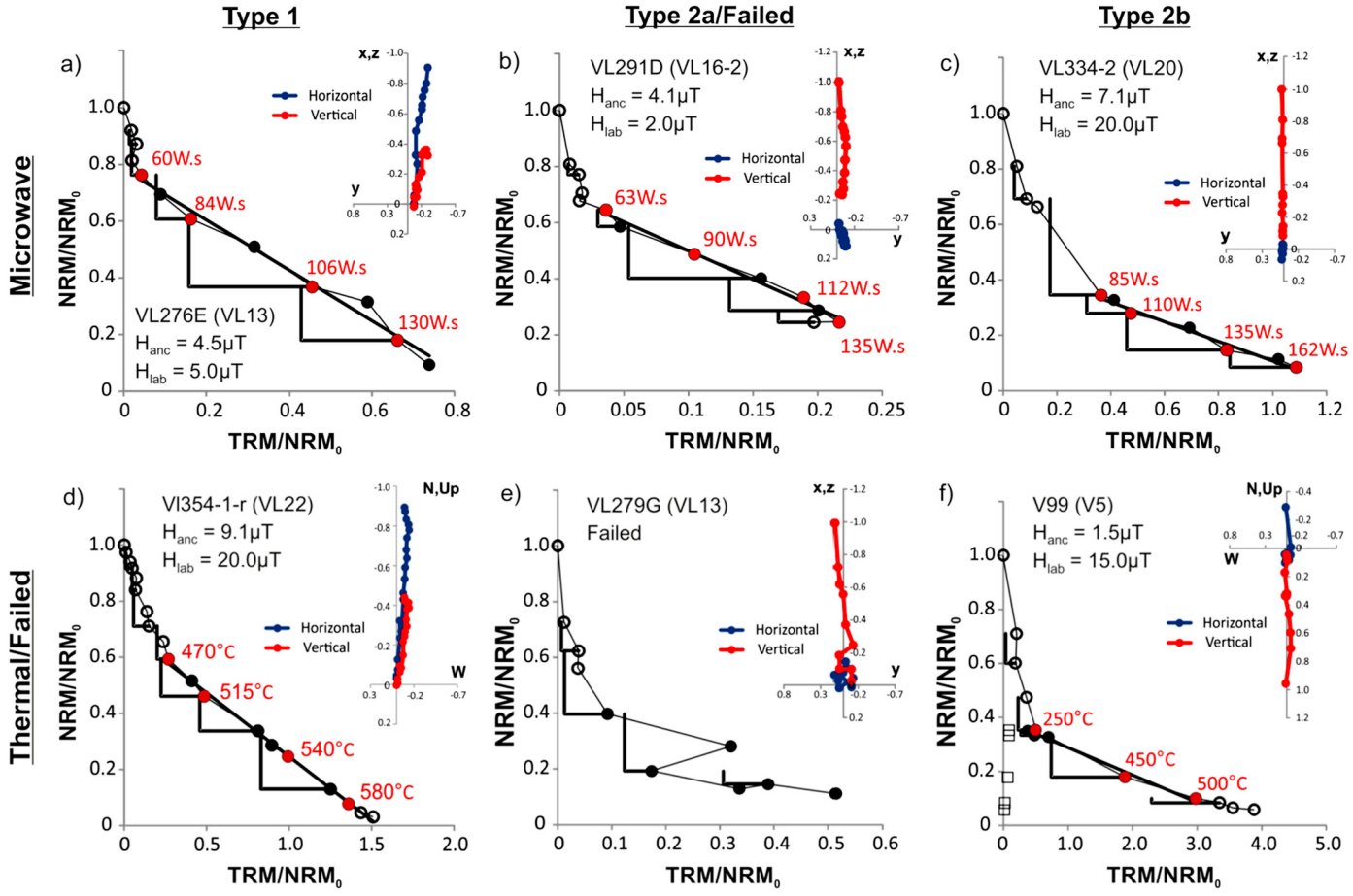

Fig. 5. Example Arai plots illustrating the two experimental protocols; top row (a, b, c) are Microwave IZZI protocol and the bottom row (d, f) are Thermal Thellier-type. The Arai plots also illustrate the behaviour of the three different magnetic mineralogy types; first column (a, d) are Type 1, second column (b) is Type 2a and the third column (c, f) are Type 2b. There are no thermal examples of Type 2a magnetic mineralogy that passes; e) is a typical example of a failed (Microwave IZZI protocol) Arai plot showing zig-zagging and failed pTRM checks. All show the two-slope appearance typical for these samples. An example of an Arai plot displaying a distinct overprint, from site V7 is in Fig. 8b.

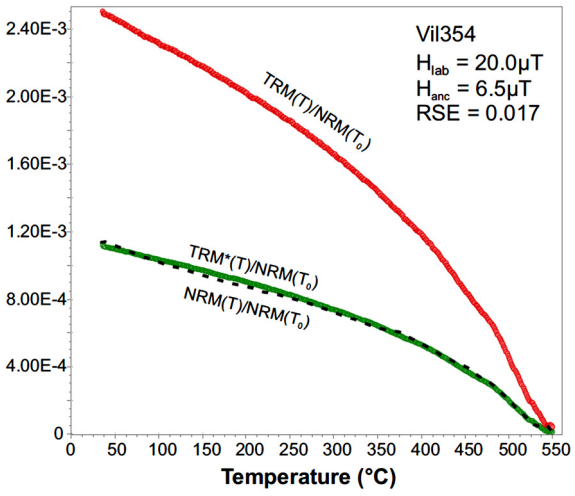

Fig. 6. Typical example of a thermomagnetic curve for the Wilson method; – the thermomagnetic curves NRM(T), TRM(T) and TRM*(T) (the solid lines and the dashed line, respectively).

tive of MD behaviour (for the Thellier–Coe the slope is curved and doesn't pass k') and the samples alter too early in the experiment, as seen by failure of the pTRM checks towards the end of the experiment. As all of the samples came from unoriented blocks, it's not possible to check the paleodirections from the paleointensity experiments; however the results from the thermal Thellier–Coe experiments are within the temperature ranges used for the paleodirections. While the relationship between the power integral and the blocking temperature is unclear, Microwave and Thermal Arai plots, for the same samples, are very similar in appearance.

4.3. Pseudo-Thellier

Non-heating pseudo-Thellier experiments (Tauxe et al., 1995) were performed to determine if the two slope nature of the Arai plots was due to thermal alteration during the palaeointensity experiment. Samples went through stepwise AF up to 100 mT using the 2G cryogenic magnetometer at the UofA, before having an ARM applied along the Z axis using the same steps and a bias field of 5–10 μT. Pseudo Arai plots were made by plotting the NRM lost against ARM acquired and vector difference sum calculations were used to remove the effect of the overprints being non-convergent. The AF demagnetisation did not resolve the two components as well as the Microwave and Thermal methods so, when calculating the ratio of the two slopes, only the points close to the start and end of the experiment were used. When compared to specimens from the same site, the Arai and Pseudo-Arai plots are very similar in shape (Fig. 7), both with the two-slope plots and site V7 which is overprinted in a different direction. The similarity in shape between the plots suggests that thermal alteration is an unlikely candidate for the two-slope plots.

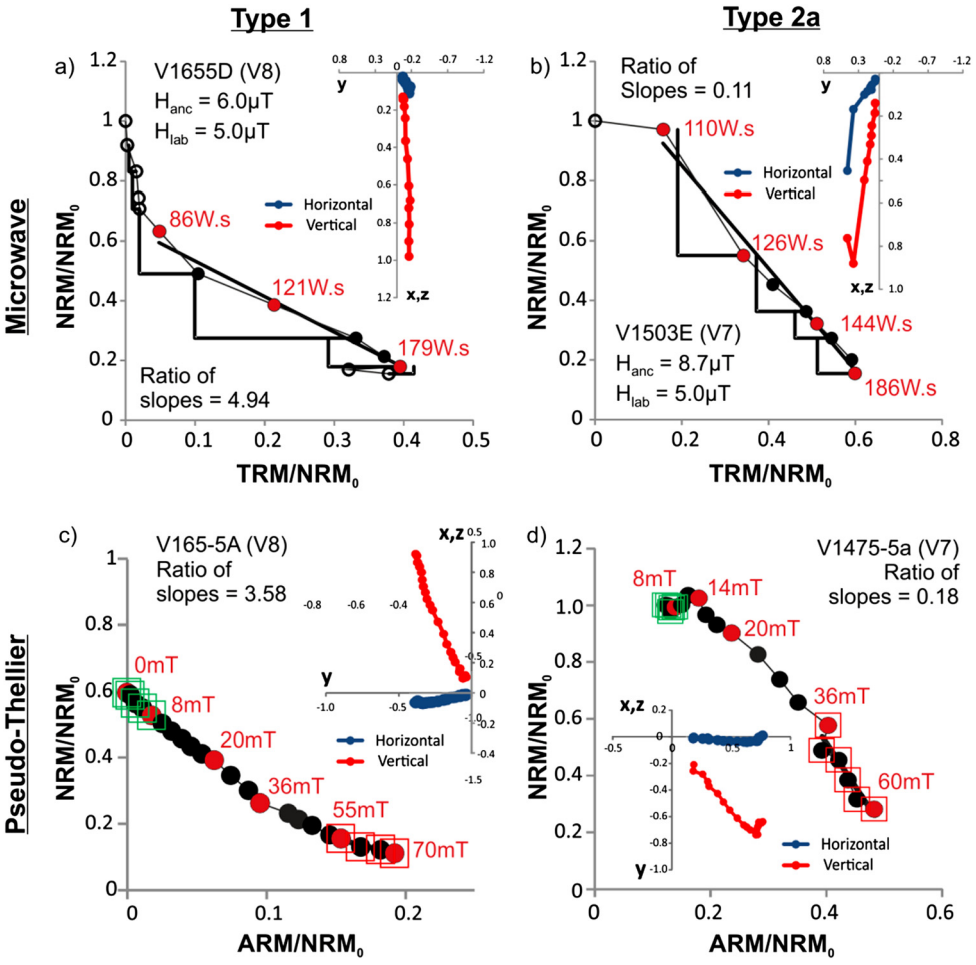

Fig. 7. Examples of Microwave IZZI protocol Arai plots (top row; a, b) and example "Arai" plots from the Pseudo-Thellier method (bottom row; c, d) from the same sites to compare with. The Arai plots represent different magnetic mineralogy types; the first column (a, c) are type 1 and the second column (b, d) are type 2a. There is no example for type 2b as none of the pseudo-Thellier plots had microwave or thermal plot with the same palaeodirectional behaviour to compare too. The ratio of slopes for both the Microwave and Pseudo-Thellier plots are given to illustrate the similarity in shape between the two methods, suggesting that the shape of the plots is not related to alteration due to heating during the Microwave and thermal paleointensity experiments.

5. Discussion

5.1. Possible causes of two-slope behaviour

The most commonly accepted causes of two-slope Arai plots that appear to be from a single paleodirectional component are a) multi-domain (MD) behaviour leading to a curved Arai plot (Dunlop and Özdemir, 2001) and b) that the second slope is produced by alteration of the magnetic mineralogy during the experiment due to heating (Kissel and Laj, 2004). Recent work by Shaar and Tauxe (2015) has shown that "aging" samples can also produce curved Arai plots due to an instability of thermoremanence, attributed to irreversible changes in the micromagnetic structures of non-SD grains. Another possibility is that the specimen is recording an overprint several times stronger than the ChRM, with an indistinguishable field direction. The correct interpretation of these Arai plots is vital because incorrectly selecting either the high or low temperature components on the curve will produce an over- or underestimate of the paleofield strength.

Laboratory-induced alteration seems to the least likely of the explanations for several reasons. The first is that the accepted results all include a sufficient number of positive pTRM checks, passing both DRAT and CDRAT selection criteria, suggesting no significant alteration has occurred. Furthermore, the two-slope behaviour is observed, and gives similar results from, all magnetic mineralogy types. This includes the type 1 samples that contain nearly pure magnetite and do not show any signs of alteration during heating during the rock magnetic experiments (Fig. 3a, b). Finally, the Pseudo-Thellier results also produce two slope Arai plots despite the samples not undergoing any heating.

It's also seems unlikely that MD behaviour or "aging" of the thermoremanence caused the two-slope behaviour exhibited by these samples. Both multi-domain behaviour and samples strongly affected by aging, based on the results from the Shaar and Tauxe (2015), tend to produce zig-zagging of the Arai and/or Zijderveld plots when IZZI protocol is used. IZZI was used for most of the experiments in this study and those that exhibited this behaviour (see Fig. 5e) were not included, while results from the Coe protocol are shown to give consistent results and/or have pTRM tail checks. Furthermore, both also cause curvature of the Arai plot and all of the selected components had to pass k' selection criteria, which checks for the curvature of the selected component.

The apparent remaining option is that the two slopes are caused by an overprint of thermal or (thermo-)viscous origin, acquired in a field of similar direction but greater field strength. The similarity in direction suggests that the overprint could have been acquired soon after the traps were emplaced. However, while the spline fit for the APW path for Siberia (Torsvik et al., 2012) suggests that north–south motion was relatively small during the Early Carboniferous ($\leq$4 cm/yr), this is based on very few data points (there is a data gap of >70 Ma either side of the 360 Ma

Table 1
Summary of site mean palaeointensity data and QPI criteria for all of the investigated sites that pass selection criteria.

Site	Lat°	Long°	Paleodirections (stratigraphic)				Magnetic mineralogy type	Paleointensity[a]								QPI criteria								QPI
			Dec°	Inc°	k	a95°		n	N_{MW}	N_{TT}	N_W	N	PI (μT)	s.d. (μT)	s.d./PI	VDM ($Z\,A\,m^2$)	AGE	STAT	TRM	ALT	MD	ACN	TECH	LITH	MAG	
V5	62.3	116.0	148.1	81.7	86.4	9.9	I/2b	11	3	1	0	4	**8.7**	4.8	55%	11.6	1	0	1	1	1	1	1	0	1	7
V7	62.3	116.1	316.2	−42.3	38.5	5.6	2a	16	5	0	0	5	**6.7**	1.7	25%	14.1	1	0	0	1	1	1	0	0	1	5
V8	62.3	116.1	154.2	68.0	142.7	3.5	1	10	6	0	0	6	**5.9**	0.9	15%	9.1	1	1	1	1	1	1	0	0	1	7
Vil 13	62.6	115.4	211.3	75.2	78.0	6.1	I/2a/2b	18	6	0	0	6	**4.7**	1.0	21%	6.6	1	0	1	1	1	1	0	0	1	6
Vil 16-1	62.6	115.4	196.0	62.8	95.8	7.9	2a	9	3	0	0	3	**14.0**	0.5	4%	23.3	1	0	0	1	1	1	0	0	1	5
Vil 16-2	62.6	115.4	184.3	59.5	50.4	10.9	2a	16	9	0	0	9	**2.5**	0.7	29%	4.3	1	0	0	1	1	1	0	0	1	5
Vil 18-1	62.6	115.4	187.1	62.7	232.3	4.4	2a	15	2	0	3	5	**2.4**	1.1	45%	4.3	1	0	0	1	1	1	1	0	1	6
Vil 20	62.3	116.0	203.3	75.9	26.1	10.1	2b	11	3	2	0	5	**10.0**	2.0	20%	14	1	0	0	1	1	1	1	0	1	6
Vil 22	62.3	116.1	215.1	76.1	142.1	3.8	1	15	0	5	3	8	**6.9**	1.7	25%	9.5	1	0	1	1	0	1	1	0	1	6

[a] n is the number of samples measured per site; N_{MW} N_{TT} N_W and N are the number of Microwave, Thellier, Wilson and the the total number of measurements that were accepted.

pole). The APW curve of Siberia, and later Baltica at ∼250 Ma, doesn't appear to go back to this latitude in the subsequent 360 Ma, although it is possible that a thermal overprint could have been acquired during a period when local field directions deviated from the average global field.

As for a (thermos-)viscous overprint, Kravchinsky et al. (2002) reported a low temperature component (LTC), present up to 300 °C, across all of the 360 Ma pole sites (including the kimberlite pipes) and in line with the regional geomagnetic field. This apparent present day overprint was reported as being significantly different from the high temperature component (HTC). However, all but one of the sites reported were reversed, while all the sites presented in this study are normal apart from V7, which shows the overprint. The LTC site means from the Orlov and Shatsillo sites, agree with the site means from the Kravchinsky et al. (2002) paper (see Supplementary Appendix C), suggesting that they carry the same overprint. We note that although the palaeointensity values associated with the LTC of 15.1–51.9 μT (21–71 $Z\,A\,m^2$) are comfortably within the range of the field observed for Eastern Asia for the past 6000 yr (Cai et al., 2017), the likely non-thermal origin of this component precludes a reliable palaeointensity.

Further evidence of a viscous overprint comes from Fig. 8, which shows the apparent direction of the acquired pTRMs for two examples where both the low and high temperature slopes pass for the same measurement (observed in type 1 samples only). In both the Microwave and Thermal cases, the LTC pTRM directions are deflected from the applied field direction, converging towards the applied field direction with increasing power/temperature steps, while the HTC pTRMs match the applied field direction. However, sequential Microwave pTRMs appear to differ by a high angle, sometimes >90°, while sequential Thermal pTRM's differ by a much smaller angle. This deflection does not appear to be the result of magnetic anisotropy as the direction is not consistent.

Instead, this behaviour appears to be due to pTRM tails. Typically, pTRM tails manifest as curved Arai plots or failed pTRM tail checks in Thellier-type experiments using the Coe protocol and zig-zagging Arai and/or Zijderveld plots for those using IZZI. Curved or zig-zagging Arai plots and failed pTRM tail checks are due to an overall difference in the intensity between the Z and I steps. However, where zig-zagging occurs in the Zijderveld plot, but not the Arai plot, this is because the overall intensity of the pTRMs acquired and removed are equal but the vector components (x, y, z) of this gain/loss are not the same. If the applied field is quasi-perpendicular to the NRM, as recommended (Biggin et al., 2007b), and excessive unblocking occurs in the dominant component of the applied field direction (e.g. for an applied field with an inclination of ±90°, the z component is dominant), if this is not entirely removed by the Z step then this deflects the NRM direction e.g. causing Zijderveld zig-zagging.

Similar behaviour appears to deflect the pTRM directions, except that the excess unblocking occurs in a non-dominant component. For example, the applied field for V92-1D (Fig. 8a, b) had an inclination of 0° but the pTRMs acquired had a significant z component. Experiments to estimate the domain structure of the samples confirm some non-ideal behaviour in the LTC (a small pTRM tail formed at <400 °C) for Vil 354 (Supplementary Appendix D; comparable to Vil 352 in Fig. 8e–h) but SD behaviour in the HTC (no pTRM tail). Apart from plotting the apparent pTRM directions, which is not commonly done, this behaviour may be distinguishable from Υ (the angular distance between applied field and pTRM directions; Paterson et al., 2014). In the majority of cases, Υ is high for the LTC s ($\gg 5°$) and low for the HTC ($\leq 5°$) but this is not always the case (see Supplementary Appendix A; site V5 for an example where this is true and site Vil 13 for a case where there is a LTC with a low Υ and a HTC with a high Υ).

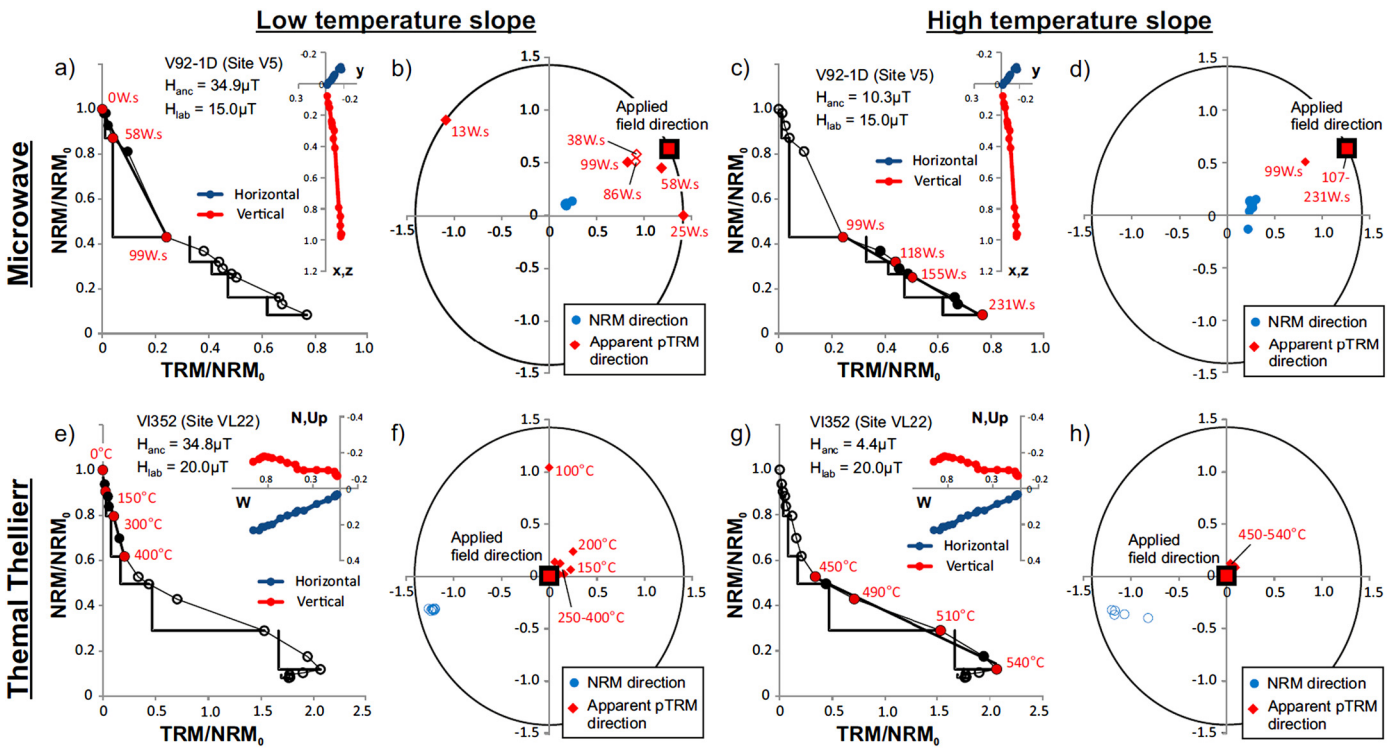

Fig. 8. Examples of two-slope Arai plots, where both slopes pass selection criteria, with stereoplots showing the NRM direction of the sample and apparent pTRM directions. The samples both have Type 1 mineralogy, the only mineralogy where both slopes from the same experiment are shown to pass. The top row is a Microwave IZZI protocol example showing; a, b) the low temperature slope and c, d) high temperature slope. The bottom row is a Thermal Thellier–Coe example showing; e, f) the low temperature slope and g, h) high temperature slope. While the NRM directions do not vary significantly across the two slopes, the pTRM checks for the low temperature slope are deflected from the applied field direction; in both cases they tend toward the applied field direction with increasing power/temperature steps. The deflection of the pTRM's is not in a consistent direction, which excludes magnetic anisotropy as the cause, leaving pTRM tails as a likely explanation. For the Microwave experiment, sequential pTRM's look to differ by a high angle, sometimes >90°, while sequential Thermal pTRM's differ by a much smaller angle. This could be due to the different protocols, with the high angle caused because of the alternating ZI and IZ steps used during the Microwave experiments. This deflection of the pTRM directions is representative of all of the low temperature pTRM behaviour observed across the different sites and magnetic mineralogy types, which is why all of the LTC's have been excluded even if they passed selection criteria.

5.2. Reliability of the paleointensity results

To evaluate the reliability of the sites, Q_{PI} criteria (Biggin and Paterson, 2014) were applied to the 9 sites that passed selection criteria. All the sites meet the AGE criterion due to the isotopic age dating, in agreement with the stratigraphy, and paleodirections consistent with APW. Only one of the sites meets the STAT criterion, some most likely failing because of the low site means. TRM has been awarded to all of the sites with Type 1 mineralogy as the SEM results show primary igneous textures with no evidence of maghematisation and to site Vil 13 because the different mineralogy's give consistent results. All of the sites pass ALT because the experiments use pTRM checks and pass DRAT and CDRAT. All sites, apart from Vil 22, pass MD by using a combination of one or more of the following; IZZI protocol without zig-zagging in the Arai or the Zijderveld plots (Microwave experiments), pTRM tails with DRATtail $\leq$10% (Thermal Thellier–Coe experiments) or use a domain-state independent method (Wilson technique). All of the sites pass ACN; anisotropy effects have been ruled out because the pTRM deflection at low temperatures/powers is inconsistent and the Υ values for the HTC are low (see Supplementary Appendix A), low field values were applied ($\leq$20 μT) to negate the non-linear TRM effects and the magnetic grains appear PSD in size so cooling rate effects should be negligible (Biggin et al., 2013). Four out of the nine sites met TECH by using more than one palaeointensity technique, all the sites fail LITH as they sample a single lithology and all of the sites pass MAG because the measurement data has been made publically available (Supplementary Appendix E). Based on the current criteria definitions, all of the sites score highly (5–7), suggesting that the data is reliable.

The site mean paleointensities range from 2.4–14 μT, giving VDM values of 4.3–23.3 ZAm^2; the locality mean field strength is 6.9 μT or 10.9 ZAm^2. Fig. 9 shows the results from this study, along with the other recent Siberian results from Minusa and Kola (Shcherbakova et al., 2017) and the Devonian–Carboniferous results from the 2015 PINT database (Biggin et al., 2009) and the World Paleointensity Database (wwwbrk.adm.yar.ru/palmag/database_e.html). The Viluy results are in close agreement with those from Minusa (site mean for the most reliable, green and yellow sites is 30.7 ZAm^2) and even closer agreement with Kola (site mean of 10.5 ZAm^2), which potentially overlaps in age with the Viluy samples (Viluy samples are age dated to between 363–378 Ma, Kola to between 371–387 Ma). The Viluy results are also in close agreement with most of the other Devonian–Carboniferous sites, despite their questionable reliability; many of the site results come exclusively from non-Thellier methods and all were taken before modern selection criteria were in place e.g. in many cases the experiments do not have any of the standard checks for alteration (pTRM checks) or MD behaviour (pTRM tails checks/IZZI protocol). The combination of all of these results gives strength to the argument that the Devonian field was significantly weaker than the average Phanerozoic geomagnetic field; between 42 ZAm^2 (Tauxe et al., 2013) and 50 ZAm^2 (Biggin et al., 2015).

However, these average field strengths are significantly weaker than the expected dipole based on the past few million years (Cromwell et al., 2015) and there are several possibilities for why these results could underestimate field strength that may not fully

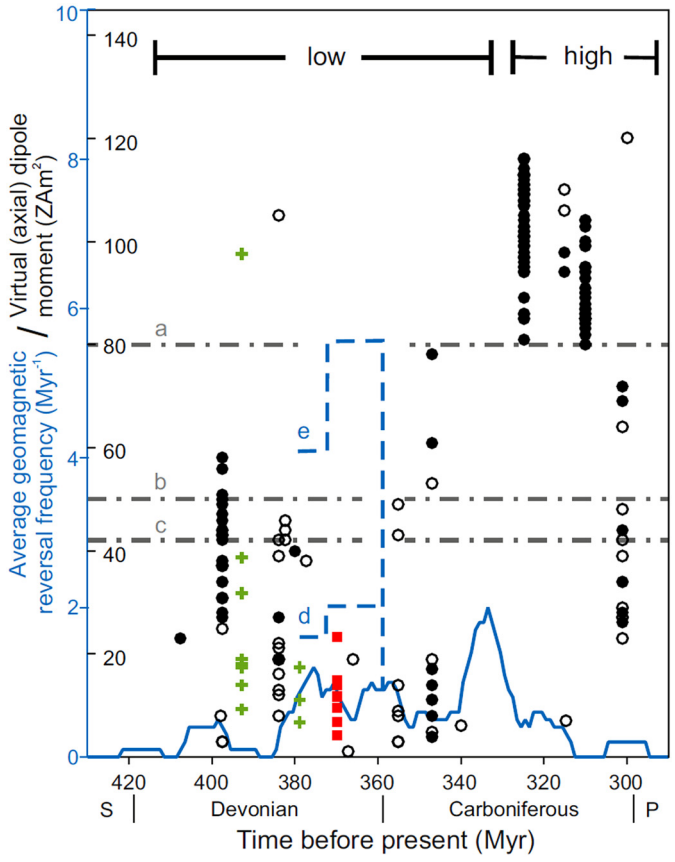

Fig. 9. V(A)DM values for the Devonian–Carboniferous sites (black circles; filled have $n \geq 3$ and std. dev $\leq$25%) from the PINT15 database (Biggin et al., 2009) and the World Paleointensity Database (wwwbrk.adm.yar.ru/palmag/database_e.html), with recently published data from Minusa and Kola (green crosses) and Viluy data published here (red squares). The blue line represents the average reversal frequency binned per 10 million yr (unbroken line represents the schematic Canning Basin from the GTS2016 update, which is likely to be an underestimate, and the dashed blue lines are for the d) minimum and e) maximum possible reversal frequency from Hansma et al., 2015). The dashed grey lines represent average field strength for a) the present day and the Phanerozoic average field strength from b) Biggin et al. (2015) and c) Tauxe et al. (2013).

be evaluated by the Q_{PI} criteria; a) not averaging the global field, b) thermo-chemical remanent magnetisation (TCRM) and c) non-SD behaviour. As discussed in Section 2, while it is not entirely clear if the Emyaksinsk Formation (the Vil sites) covers paleosecular variation, and the majority of the results do come from this section (6 out of the 9 sites), the combination of the sites should reasonably cover palaeosecular variation ($k = 25.4$ and V7 is reversed compared to the other sites) and the average of the Vil sites is only slightly weaker than the average for the V sites (10.3 ZA m^2 instead of 11.6 ZA m^2). Non-dipolar field behaviour or APW between sites would also affect the interpretation of the results but there is little evidence of these from the age dating and paleodirections.

TCRM acquisition is generally considered to be less efficient than TRM acquisition but can produce linear slopes, meaning any palaeointensity results could pass selection criteria but are likely to underestimate the past field strength (Fabian, 2009). There are two forms of TCRM acquisition that could affect these samples, either low or high temperature oxidation (e.g. maghematisation and oxyexsolution respectively). The best indication of the possible effects of maghematisation comes from Vil 13, which includes samples of all three magnetic mineralogy types. The samples all gave very consistent results, with the site just missing out on STAT (probably because of the low site mean <5 μT), suggesting that the maghematisation has not had a significant impact on the paleointensity estimates. For this reason, the sites have been included, though they are less reliable (illustrated by the failed TRM criterion). By removing all of the Type 2 samples, the overall mean remains relatively unchanged (10.1 ZA m^2 instead of 10.8 ZA m^2) but the standard deviation reduces (3.3 ZA m^2 instead of 6.0 ZA m^2). However, it is unclear whether this is due to the effects of the mineralogy or if the inclusion of the Type 2 sites produces a better sampling of the paleosecular variation. As for oxyexsolution, while it is been observed in these samples and it has been suggested as a possible cause of low field estimates (Smirnov and Tarduno, 2005), it is generally accepted that oxyexsolution occurs at temperatures not much lower than 600 °C (Dunlop and Özdemir, 1997) and the HTC starts unblocking at a much lower temperature than in the Smirnov and Tarduno study, so any TCRM from oxyexsolution is unlikely to be a significant part of the ChRM.

Non-SD behaviour of the remanence carriers has also been suggested as a possible reason for why the Phanerozoic field appears weaker than expected; either due to MD behaviour causing Arai plot curvature (Smirnov et al., 2017) or due to the instability of the thermoremanence over time (Shaar and Tauxe, 2015). However, it is not uncommon for samples older than these to have the ChRM from two-slope Arai plots accepted, even if the overprint direction are indistinguishable, while the low temperature slope is dismissed as being carried by MD to large PSD grains (Kulakov et al., 2013). Section 5.1 outlines the evidence for non-SD behaviour affecting the LTC, but not the HTC. While it is still possible that non-SD behaviour, if present, may be exaggerating the curvature of the Arai plot, the (thermo-)viscous overprint is clearly causing the two-slope appearance. Also, apart from the large titanomaghemite grains of the type 2b samples (only 20% of the accepted results), all of the magnetic recorders appear to be on the smaller size of PSD, which has been shown to magnetically stable for billions of years (Almeida et al., 2014).

5.3. Implications of a weak Devonian field

As discussed in section 1, results from models suggest that when the dipole moment is small, an increase in the reversal frequency and the non-dipolar components of the field are expected. This agrees with the most recent estimates in reversal frequency for the Upper Devonian of ~2–5 Myr^{-1} by Hansma et al. (2015) based on the Oscar Range stratigraphy (see the minimum and maximum reversal frequencies represented by the blue dashed lines in Fig. 9). This is especially true if this is, as suggested by the authors, potentially an underestimate due to under sampling. There is not much evidence to support this from the Viluy HTC directions, although the "strange" directions (e.g. previously unpublished V sites) could be suggestive of non-GAD behaviour. However, other Devonian age Siberian sites, including the Minusa sites (Shcherbakova et al., 2017), the Zharovsk complex (Shatsillo et al., 2014) and Appainskaya Suite (Konstantinov et al., 2016) all indicate a range of ChRM components that could relate to an increase in the non-dipolar component.

The low field values, and potentially high reversal frequency/larger multi-polar component, may suggest that convection in the outer core was more vigorous during this period (Olson, 2007), probably caused by an increase in the total heat flow across the core–mantle boundary (CMB) or changes in its pattern (Olson and Amit, 2014). Variation in heat flow across the CMB is driven by changes in the structure of the deep mantle (relative to the core) due to plumes, slabs, distribution of deep basal piles and True Polar Wander (TPW; Biggin et al., 2012). Due to the limitations of plate reconstructions for the Devonian, it is difficult to determine the influence of these different components, especially the degree and influence of subduction and TPW. The easiest to es-

timate is plume activity by looking at the distribution of LIP's emplaced after this time although this will be negatively affected by preservation bias. There may have been an increase in the number of LIP's emplaced approximately ~50 Myr after the Viluy LIP (Biggin et al., 2012), which could reflect the time it takes a plume to rise through the mantle. The Viluy LIP has also been suggested as one of the causes of the Frasnian–Famemnian extinction event (Kravchinsky et al., 2002) but we note the suggestion of Shcherbakova et al. (2017) that a sustained weak and nondipolar field in the mid-Palaeozoic would cause a long-term reduction in the effective shielding of the magnetosphere, potentially also affecting the biosphere. The veracity of claimed links between geomagnetic field behaviour and deep Earth, as well as biological, evolution remains to be elucidated.

6. Conclusions

New data from the Upper Devonian Viluy LIP show the field to be significantly weaker than the average Phanerozoic field, in close agreement with recent, Lower Devonian results from the Minusa Basin, Siberia and the Kola Peninsula. The weak field values, along with moderate to high reversal frequencies and a potentially significant multipolar component, suggest convection in the core was more vigorous during the Devonian, which may relate to increased heat flow across the CMB due to a high level of LIP producing plume activity at this time. This field behaviour preceding the PCRS is also similar to that prior to the two other Superchrons during the Phanerozoic, implying this sharp transition in behaviour may relate to the initiation of the Superchron.

This study also shows that variable slope Arai plots can be considered for paleointensity with appropriate stipulations; the nature of both slopes needs to be confirmed and caution should be taken as not all non-SD behaviour is apparent from conventional paleointensity selection criteria. Generally this type of pTRM tails results in a high Υ, while the component unaffected by tails has a low Υ value; however, this is not evident in all of the cases so there is an argument for plotting the apparent pTRM directions.

Acknowledgements

This work was supported NERC DTP Studentship (1511981). VVS acknowledges support from RFBR grant 16-05-446-a. AJB acknowledges support from The Leverhulme Trust (RL-2016-80) and NERC (NE/P00170X/). VAK and TA acknowledge the Natural Sciences and Engineering Research Council of Canada (NSERC) grant (RGPIN-2014-04183). VEP and AVP were supported by grant 14.Z50.31.0017 of the Government of the Russian Federation.

Appendix A. Supplementary material

Supplementary material related to this article can be found online at https://doi.org/10.1016/j.epsl.2018.10.035.

References

Almeida, T.P., Kasama, T., Muxworthy, A.R., Williams, W., Nagy, L., Dunin-Borkowski, R.E., 2014. Observing thermomagnetic stability of nonideal magnetite particles: good paleomagnetic recorders? Geophys. Res. Lett. 41, 7041–7047. https://doi.org/10.1002/2014GL061432.

Biggin, A.J., Badejo, S., Hodgson, E., Muxworthy, A.R., Shaw, J., Dekkers, M.J., 2013. The effect of cooling rate on the intensity of thermoremanent magnetization (TRM) acquired by assemblages of pseudo-single domain, multidomain and interacting single-domain grains. Geophys. J. Int. 193, 1239–1249.

Biggin, A.J., Paterson, G.A., 2014. A new set of qualitative reliability criteria to aid inferences on palaeomagnetic dipole moment variations through geological time. Front. Earth Sci. 2, 1–9. https://doi.org/10.3389/feart.2014.00024.

Biggin, A., Perrin, M., Dekkers, M., 2007a. A reliable absolute palaeointensity determination obtained from a non-ideal recorder. Earth Planet. Sci. Lett. 257, 545–563. https://doi.org/10.1016/j.epsl.2007.03.017.

Biggin, A., Perrin, M., Shaw, J., 2007b. A comparison of a quasi-perpendicular method of absolute palaeointensity determination with other thermal and microwave techniques. Earth Planet. Sci. Lett. 257, 564–581. https://doi.org/10.1016/j.epsl.2007.03.016.

Biggin, A.J., Piispa, E.J., Pesonen, L.J., Holme, R., Paterson, G.A., Veikkolainen, T., Tauxe, L., 2015. Palaeomagnetic field intensity variations suggest mesoproterozoic inner-core nucleation. Nature 526, 245–248. https://doi.org/10.1038/nature15523.

Biggin, A.J., Steinberger, B., Aubert, J., Suttie, N., Holme, R., Torsvik, T.H., van der Meer, D.G., van Hinsbergen, D.J.J., 2012. Possible links between long-term geomagnetic variations and whole-mantle convection processes. Nat. Geosci. 5, 526–533. https://doi.org/10.1038/ngeo1521.

Biggin, A.J., Strik, G.H.M.A., Langereis, C.G., 2009. The intensity of the geomagnetic field in the late-Archaean: new measurements and an analysis of the updated IAGA palaeointensity database. Earth Planets Space 61, 9–22. https://doi.org/10.1186/BF03352881.

Cai, S., Jin, G., Tauxe, L., Deng, C., Qin, H., Pan, Y., Zhu, R., 2017. Archaeointensity results spanning the past 6 kiloyears from eastern China and implications for extreme behaviors of the geomagnetic field. Proc. Natl. Acad. Sci. USA 114, 39–44. https://doi.org/10.1073/pnas.1616976114.

Coe, R.S., 1967. The determination of paleo-intensities of the Earth's magnetic field with emphasis on mechanisms which could cause non-ideal behavior in Thellier's method. J. Geomagn. Geoelectr. 19, 157–179. https://doi.org/10.5636/jgg.19.157.

Courtillot, V., Kravchinsky, V.A., Quidelleur, X., Renne, P.R., Gladkochub, D.P., 2010. Preliminary dating of the Viluy traps (eastern Siberia): eruption at the time of late Devonian extinction events? Earth Planet. Sci. Lett. 300, 239–245. https://doi.org/10.1016/j.epsl.2010.09.045.

Cromwell, G., Tauxe, L., Halldõrsson, S.A., 2015. New paleointensity results from rapidly cooled Icelandic lavas: implications for Arctic geomagnetic field strength. J. Geophys. Res., Solid Earth 120, 2913–2934. https://doi.org/10.1002/2014JB011828.

Dunlop, D.J., 2002. Theory and application of the Day plot (Mrs/Ms versus Hcr/Hc), 1: theoretical curves and tests using titanomagnetite data. J. Geophys. Res., Solid Earth 107.

Dunlop, D.J., Özdemir, Ö., 1997. Rock Magnetism: Fundamentals and Frontiers. Cambridge Studies in Magnetism, vol. 3. Cambridge University Press, Cambridge.

Dunlop, D.J., Özdemir, Ö., 2001. Beyond Néel's theories: thermal demagnetization of narrow-band partial thermoremanent magnetizations. Phys. Earth Planet. Inter. 126, 43–57. https://doi.org/10.1016/S0031-9201(01)00243-6.

Fabian, K., 2009. Thermochemical remanence acquisition in single-domain particle ensembles: a case for possible overestimation of the geomagnetic paleointensity. Geochem. Geophys. Geosyst. 10. https://doi.org/10.1029/2009GC002420. n/a–n/a.

Hansma, J., Tohver, E., Yan, M., Trinajstic, K., Roelofs, B., Peek, S., Slotznick, S.P., Kirschvink, J., Playton, T., Haines, P., Hocking, R., 2015. Late Devonian carbonate magnetostratigraphy from the Oscar and Horse Spring Ranges, Lennard Shelf, Canning basin, Western Australia. Earth Planet. Sci. Lett. 409, 232–242. https://doi.org/10.1016/j.epsl.2014.10.054.

Hill, M.J., Shaw, J., 1999. Palaeointensity results for historic lavas from Mt Etna using microwave demagnetization/remagnetization in a modified Thellier-type experiment. Geophys. J. Int. 139, 583–590. https://doi.org/10.1046/j.1365-246x.1999.00980.x.

Hill, M.J., Shaw, J., 2007. The use of the "Kono perpendicular applied field method" in microwave palaeointensity experiments. Earth Planets Space 59.

Ingham, E., Heslop, D., Roberts, A.P., Hawkins, R., Sambridge, M., 2014. Is there a link between geomagnetic reversal frequency and paleointensity? A Bayesian approach. J. Geophys. Res., Solid Earth 119, 5290–5304. https://doi.org/10.1002/2014JB010947.

Kiselev, A.I., Ernst, R.E., Yarmolyuk, V.V., Egorov, K.N., 2012. Radiating rifts and dyke swarms of the middle Paleozoic Yakutsk plume of eastern Siberian craton. J. Asian Earth Sci. 45, 1–16. https://doi.org/10.1016/j.jseaes.2011.09.004.

Kissel, C., Laj, C., 2004. Improvements in procedure and paleointensity selection criteria (PICRIT-03) for Thellier and Thellier determinations; application to Hawaiian basaltic long cores. Phys. Earth Planet. Inter. 147, 155–169. https://doi.org/10.1016/j.pepi.2004.06.010.

Konstantinov, K.M., Tomshin, M.D., Ibragimov, S.Z., Khuzin, M.Z., Konstantinov, I.K., Yakovlev, A.A., Artemova, E.V., 2016. Petro- and paleomagnetic studies of basalts of the upper Devonian Appainskaya Suite (Western Yakutia). Geodyn. Tectonophys. 7, 593–623. https://doi.org/10.5800/GT-2016-7-4-0224.

Koymans, M.R., Langereis, C.G., Pastor-Galán, D., van Hinsbergen, D.J.J., 2016. Paleomagnetism.org: an online multi-platform open source environment for paleomagnetic data analysis. Comput. Geosci. 93. https://doi.org/10.1016/j.cageo.2016.05.007.

Kravchinsky, V.A., Konstantinov, K.M., Courtillot, V., Savrasov, J.I., Valet, J.-P., Cherniy, S.D., Mishenin, S.G., Parasotka, B.S., 2002. Palaeomagnetism of East Siberian traps and kimberlites: two new poles and palaeogeographic reconstructions at about 360 and 250 Ma. Geophys. J. Int. 148, 1–33. https://doi.org/10.1046/j.0956-540x.2001.01548.x.

Kulakov, E.V., Smirnov, A.V., Diehl, J.F., 2013. Absolute geomagnetic paleointensity as recorded by ∼1.09 Ga lake shore traps (Keweenaw Peninsula, Michigan). Stud. Geophys. Geod. 57, 565–584. https://doi.org/10.1007/s11200-013-0606-3.

Masaitis, V.L., Mikhailov, V.V., Selivanovskaya, T.V., 1975. Volcanism and Tectonics of Patom–Vylyu Middle Paleozoic Aulacogen. Nedra, Moscow.

McFadden, P.L., McElhinny, M.W., 1990. Classification of the reversal test in palaeomagnetism. Geophys. J. Int. 103. https://doi.org/10.1111/j.1365-246X.1990.tb05683.x.

Muxworthy, A.R., 2010. Revisiting a domain-state independent method of palaeointensity determination. Phys. Earth Planet. Inter. 179. https://doi.org/10.1016/j.pepi.2010.01.003.

Ogg, J.G., Ogg, G., Gradstein, F.M., 2016. A Concise Geologic Time Scale 2016 [Electronic book]. Online access with subscription: ScienceDirect Freedom Collection. Elsevier.

Olson, P., 2007. Gravitational dynamos and the low-frequency geomagnetic secular variation. Proc. Natl. Acad. Sci. USA 104, 20159–20166. https://doi.org/10.1073/pnas.0709081104.

Olson, P., Amit, H., 2014. Magnetic reversal frequency scaling in dynamos with thermochemical convection. Phys. Earth Planet. Inter. 229, 122–133. https://doi.org/10.1016/j.pepi.2014.01.009.

Orlov, S., Shatsillo, A.V., 2011. Paleomagnetic data on the middle Paleozoic magmatic complex from Appainskoi and Emaksinskoi suites, Yggyatinskoi depression (Siberian platform). In: Proceedings of Conference on Paleo- and Rock-Magnetism. Borok.

Paterson, G.A., 2011. A simple test for the presence of multidomain behavior during paleointensity experiments. J. Geophys. Res., Solid Earth 116. https://doi.org/10.1029/2011JB008369.

Paterson, G.A., Tauxe, L., Biggin, A.J., Shaar, R., Jonestrask, L.C., 2014. On improving the selection of Thellier-type paleointensity data. Geochem. Geophys. Geosyst. 15, 1180–1192. https://doi.org/10.1002/2013GC005135.

Pavlov, V., Gallet, Y., 2005. A third superchron during the Early Paleozoic. Episodes 28, 78–84.

Pavlov, V., Gallet, Y., 2001. Middle Cambrian high magnetic reversal frequency (Kulumbe river section, northwestern Siberia) and reversal behaviour during the Early Palaeozoic. Earth Planet. Sci. Lett. 185, 173–183. https://doi.org/10.1016/S0012-821X(00)00364-2.

Ricci, J., Quidelleur, X., Pavlov, V., Orlov, S., Shatsillo, A., Courtillot, V., 2013. New 40Ar/39Ar and K–Ar ages of the Viluy traps (Eastern Siberia): further evidence for a relationship with the Frasnian–Famennian mass extinction. Palaeogeogr. Palaeoclimatol. Palaeoecol. 386, 531–540. https://doi.org/10.1016/j.palaeo.2013.06.020.

Riisager, P., Riisager, J., 2001. Detecting multidomain magnetic grains in Thellier palaeointensity experiments. Phys. Earth Planet. Inter. 125. https://doi.org/10.1016/S0031-9201(01)00236-9.

Shaar, R., Tauxe, L., 2015. Instability of thermoremanence and the problem of estimating the ancient geomagnetic field strength from non-single-domain recorders. Proc. Natl. Acad. Sci. USA 112, 11187–11192. https://doi.org/10.1073/pnas.1507986112.

Shatsillo, A.V., Fedyukin, I.V., Powerman, V.I., 2014. Paleomagnetism of the Late Paleozoic granites of the Angara–Vitim batholith and the host rocks of the Baikal–Patom folded area: tectonic implications. Russ. Geol. Geophys. 55, 864–880. https://doi.org/10.1016/j.rgg.2014.06.006.

Shcherbakova, V.V., Biggin, A.J., Veselovskiy, R.V., Shatsillo, A.V., Hawkins, L., Shcherbakov, V.P., Zhidkov, G.V., 2017. Was the Devonian geomagnetic field dipolar or multipolar? Palaeointensity studies of Devonian igneous rocks from the Minusa Basin (Siberia) and the Kola Peninsula dykes, Russia. Geophys. J. Int. 209, 1265–1286. https://doi.org/10.1093/gji/ggx085.

Shpount, B.R., Oleinikov, B.V., 1987. A comparison of mafic dike swarms from the Siberian and Russian platforms. In: Halls, H.C., Fahrig, W.F. (Eds.), Mafic Dyke Swarms. Geological Association of Canada, St. Johns, pp. 179–192.

Smirnov, A.V., Kulakov, E.V., Foucher, M.S., Bristol, K.E., 2017. Intrinsic paleointensity bias and the long-term history of the geodynamo. Sci. Adv. 3. https://doi.org/10.1126/sciadv.1602306.

Smirnov, A.V., Tarduno, J.A., 2005. Thermochemical remanent magnetization in Precambrian rocks: are we sure the geomagnetic field was weak? J. Geophys. Res., Solid Earth 110, 1–12. https://doi.org/10.1029/2004JB003445.

Tauxe, L., Gee, J.S., Steiner, M.B., Staudigel, H., 2013. Paleointensity results from the Jurassic: new constraints from submarine basaltic glasses of ODP site 801C. Geochem. Geophys. Geosyst. 14, 4718–4733. https://doi.org/10.1002/ggge.20282.

Tauxe, L., Pick, T., Kok, Y.S., 1995. Relative paleointensity in sediments: a Pseudo-Thellier Approach. Geophys. Res. Lett. 22, 2885–2888. https://doi.org/10.1029/95GL03166.

Tauxe, L., Staudigel, H., 2004. Strength of the geomagnetic field in the Cretaceous Normal Superchron: new data from submarine basaltic glass of the Troodos Ophiolite. Geochem. Geophys. Geosyst. 5. https://doi.org/10.1029/2003GC000635.

Torsvik, T.H., Van der Voo, R., Preeden, U., Mac Niocaill, C., Steinberger, B., Doubrovine, P.V., van Hinsbergen, D.J.J., Domeier, M., Gaina, C., Tohver, E., Meert, J.G., McCausland, P.J.A., Cocks, L.R.M., 2012. Phanerozoic polar wander, palaeogeography and dynamics. Earth-Sci. Rev. 114, 325–368. https://doi.org/10.1016/j.earscirev.2012.06.007.

Wilson, R.L., 1961. The thermal demagnetization of natural magnetic moments in rocks. Geophys. J. R. Astron. Soc. 5. https://doi.org/10.1111/j.1365-246X.1961.tb02928.x.

Yu, Y., Tauxe, L., 2005. Testing the IZZI protocol of geomagnetic field intensity determination. Geochem. Geophys. Geosyst. 6. https://doi.org/10.1029/2004GC000840.